World Journal of Engineering Research
Print ISSN: 2959-9865
Online ISSN: 2959-9873
DOI: https://doi.org/10.61784/wjer3131

THE TWO-LAYER ENERGY MANAGEMENT AND DISPATCH MODEL FOR MICROGRID HYBRID ENERGY STORAGE SYSTEMS BASED ON MPC

Bo Ma, Yong Liu*, WanFei Tang, Shuang Xu
Yinchuan College of Energy, Yinchuan 750001, Ningxia, China.
**Corresponding Author: Yong Liu*

Abstract: As the penetration of distributed photovoltaic (PV) and wind generation in microgrids continues to rise, the strong stochasticity of renewable output and load poses significant challenges to the economic operation of microgrids, while the lifetime degradation of energy storage batteries under frequent charging and discharging further inflates the whole-life-cycle cost of the system. To address this issue, this paper proposes a two-layer energy management and dispatch model for microgrid hybrid energy storage systems (HESS) based on model predictive control (MPC). The upper layer is an economic dispatch layer, which minimizes the sum of the electricity purchase cost and the battery degradation cost and adopts a 48-step receding-horizon optimization to determine hourly reference plans for battery charging/discharging and grid interaction; the degradation cost is modeled as a depth-quadratic function of the half-cycle throughput and of the lifetime parameters, thereby internalizing lifetime loss into the economic objective. The lower layer is a power smoothing layer, which tracks the upper-layer reference over a 12-step short horizon and exploits the fast response of the supercapacitor to smooth the high-frequency power fluctuations induced by renewable forecasting errors. A 48-hour closed-loop simulation is carried out using real hourly data containing PV and wind generation together with a real-time price series. The results show that the upper-layer dispatch achieves peak shaving and valley filling by charging at low prices and discharging at high prices, with a correlation coefficient of −0.620 between the electricity price and the grid interaction power; the battery state of charge (SOC) operates strictly within the safe range of [10%, 90%] throughout, with zero violations. Compared with the baseline strategy that ignores degradation, the degradation-aware strategy reduces the cumulative battery throughput by 44.0%, the standard deviation of power fluctuations by 32.1%, and the total cost by 6.2%. At a 40% forecasting-error level, the lower-layer supercapacitor raises the reduction in the root-mean-square battery power ramp to 41.2%, and the smoothing benefit becomes more pronounced as the forecasting error increases. The proposed model provides a feasible hierarchical scheduling approach for the optimal operation of microgrids with HESS, balancing operational economy and storage lifetime under uncertainty.
Keywords: Microgrid; Hybrid energy storage system; Model predictive control; Two-layer energy management; Degradation cost; Receding-horizon optimization

1 INTRODUCTION

1.1 Research Background and Significance

As a small power supply and distribution system that integrates distributed generators, energy storage devices and local loads, the microgrid is an important vehicle for the integration and local consumption of a high share of renewable energy. In a typical grid-connected microgrid, PV and wind power become the main sources owing to their cleanliness and low marginal cost, yet their output is strongly modulated by the diurnal cycle, season and weather conditions. Taking the real operating data used in this paper as an example, PV output is zero at 58.2% of all 744 hourly samples, exhibiting pronounced diurnal intermittency, whereas wind output is zero at only 1.6% of the samples and fluctuates continuously, forming a certain temporal complementarity with PV. Such stochasticity, intermittency and volatility of renewable output make it difficult to maintain the power balance inside the microgrid by source-side regulation alone; energy storage and the main grid must be coordinated.

Energy storage systems play multiple roles in microgrids, including peak shaving and valley filling, fluctuation smoothing and electricity price arbitrage. However, as the most widely deployed electrochemical storage, lithium-ion batteries are highly sensitive in cycle life to the depth of discharge and throughput, and frequent, deep charging and discharging markedly accelerates capacity fade. If dispatch is driven solely by minimizing the purchase cost, the optimizer tends to over-use the battery to chase price spreads, at the cost of faster lifetime loss. The data used in this paper show that the peak-to-valley ratio of the electricity price reaches 14.58, far exceeding the load peak-to-valley ratio of 3.43, which implies an extremely strong economic incentive for price arbitrage; without incorporating the degradation cost into the objective, the battery is very likely to be worn out. Therefore, how to explicitly characterize and internalize the battery degradation cost in economic dispatch is one of the core questions that microgrid energy management must answer.

Furthermore, a single storage medium can hardly satisfy both the requirement of large-capacity energy scheduling and that of fast, high-frequency smoothing. Batteries have high energy density but relatively slow power response and a cycle life limited by throughput; supercapacitors have high power density, fast response and long cycle life but low energy

© By the Author(s) 2026, under the CC BY-NC-ND license (http://creativecommons.org/licenses/by-nc-nd/4.0).

density. Combining the two into a hybrid energy storage system (HESS), with the battery undertaking low-frequency energy-type tasks and the supercapacitor undertaking high-frequency power-type tasks, has become an effective way to improve overall storage performance. It is against this background that this paper investigates a two-layer energy management and dispatch method that explicitly accounts for the degradation cost for microgrids with HESS, balancing operational economy, power quality and storage lifetime, which is of clear engineering significance.

1.2 State of the Art

Extensive work has been carried out worldwide on microgrid energy management, which can be broadly grouped into three directions. The first is the evolution of optimal dispatch methods. Early studies mostly adopted deterministic optimization for the economic dispatch of microgrids, but such approaches can hardly cope with the uncertainty of renewable output; stochastic optimization and multi-scenario methods were therefore introduced. Feng et al. proposed a multi-period stochastic economic dispatch model for microgrids that accounts for renewable energy uncertainty and improved the solution efficiency with a parallel algorithm [1]. Xie et al. presented a systematic review of optimization-based power and energy management systems for shipboard microgrids, covering methods ranging from mixed-integer programming to intelligent optimization and their applicable boundaries [2]. These studies laid the fundamental framework of microgrid economic dispatch, but most of them focus on optimization at a single time scale and are relatively weak in representing real-time rolling feedback and storage lifetime.

The second direction is the application of model predictive control to energy management. Through receding-horizon optimization and feedback correction, MPC re-solves the optimization problem at each control step using the latest measurements and forecasts, which naturally matches the real-time dispatch requirements of microgrids under uncertainty [3]. Pippia et al. proposed a single-level rule-based MPC energy management method for grid-connected microgrids that reduces the online computational burden while ensuring economy [4]; Ponce et al. integrated battery energy storage dispatch into an MPC-based energy management system for a hybrid microgrid and verified the effectiveness of MPC in coordinating storage and grid interaction [5]; Nair et al. analyzed the interaction among energy storage systems within a multi-objective MPC framework for DC microgrids [6]. These studies show that MPC is a powerful tool for real-time microgrid dispatch, but a single-layer MPC can hardly address the economy at the slow time scale and the power quality at the fast time scale simultaneously.

The third direction is hybrid energy storage and hierarchical/two-layer energy management. To exploit the complementary advantages of different storage media, Liu et al. proposed a power allocation control method for an HESS composed of lithium-ion batteries and supercapacitors, in which the supercapacitor handles the high-frequency power component [7]; Chen et al. verified the role of grid-level battery energy storage in smoothing wind power fluctuations [8]. At the architectural level, Jiang et al. studied hierarchical control of a microgrid with multiple distributed generations [9], and Guo et al. proposed a hierarchical economic MPC framework for a PV-hydrogen-storage microgrid [10]. Most relevant to this paper is the two-layer energy management system for hybrid energy storage microgrids considering degradation costs proposed by Ju et al. [11], which models the battery degradation cost as a function of the depth of discharge and embeds it into a two-layer EMS; it is the core theoretical source of the methodology in this paper. However, existing two-layer EMS studies are mostly based on assumed parameters or synthetic data, and a systematic quantification of the economy and smoothing performance of degradation-aware two-layer dispatch on real long-term operating data is still lacking.

1.3 Main Work and Contributions

To address the above gaps, this paper builds and validates a degradation-aware two-layer MPC-HESS energy management and dispatch model based on a real microgrid operating dataset. The main contributions are threefold. First, a two-layer MPC framework consisting of upper-layer economic dispatch and lower-layer power smoothing is established: the upper layer minimizes the sum of the purchase and degradation costs over a 48-step hourly horizon, while the lower layer tracks the upper-layer reference over a 12-step short horizon and uses the supercapacitor to smooth high-frequency fluctuations; the two layers are coordinated across time scales through the reference power and the feedback state. Second, the battery degradation cost is explicitly modeled from the cumulative throughput and lifetime parameters and internalized into the economic objective, and the improvements of the degradation-aware strategy over the degradation-ignoring baseline are quantified in terms of throughput, power fluctuation and total cost. Third, a 48-hour closed-loop simulation is completed on real data, and the robustness of the model is verified through two tests, namely prediction-horizon sensitivity and degradation-weight sensitivity.

2 MODELING OF THE MICROGRID HYBRID ENERGY STORAGE SYSTEM

2.1 Microgrid System Structure

The grid-connected microgrid studied in this paper is formed by distributed renewable sources, local loads, a hybrid energy storage system and the point of common coupling (PCC) converging on a common bus, and its architecture is shown in Figure 1. The renewable sources include PV arrays and wind turbines, each delivering power according to its own resource conditions; the local load represents the electricity demand within the microgrid; the HESS consists of lithium-ion batteries and supercapacitors in parallel, with the battery undertaking low-frequency energy-type dispatch

tasks and the supercapacitor undertaking high-frequency power-type smoothing tasks; the microgrid exchanges power bidirectionally with the main grid through the PCC, and both purchasing and selling are settled at the real-time price.

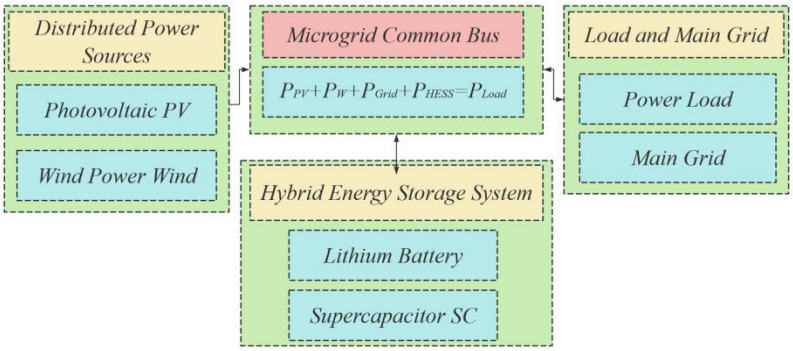


Figure 1 Architecture of the Microgrid Hybrid Energy Storage (HESS) System

As shown in Figure 1, the power balance must be satisfied at any instant: the sum of the renewable output, the net discharge power of the storage and the power injected from the grid must equal the local load. Let t denote the discrete time step, P_t^L the load power, P_t^{PV} and P_t^W the PV and wind output, P_t^b the battery charging/discharging power, P_t^{sc} the supercapacitor power and P_t^g the power injected from the grid; then the power balance can be written as:

$$P_t^g+P_t^b+P_t^{sc}+P_t^{PV}+P_t^W=P_t^L \tag{1}$$

In the upper-layer hourly economic dispatch, renewable output is aggregated into a net load to simplify the decision-making. According to the power balance setting, the net load P_t^{net} is synthesized from the load, PV and wind according to their respective conversion coefficients:

$$P_t^{net}=2P_t^L-\frac{1}{3}P_t^{PV}-P_t^W \tag{2}$$

where the conversion coefficients are derived from the capacity configuration and metering basis of the actual project. Under this formulation, the equality constraint of each upper-layer period degenerates to $P_t^g+P_t^b=P_t^{net}$, i.e. the grid power can be analytically back-substituted from the battery power, which reduces the decision dimension of each upper-layer step to the single battery power and thus facilitates efficient solution of the receding-horizon optimization.

2.2 Renewable Generation and Load Models

PV, wind and load are given as time series in this paper. The hourly series characterize the intraday supply-demand trend and serve as the input of the upper-layer economic dispatch; the real 5-minute output waveforms characterize the high-frequency fluctuations of renewable output around the hourly mean and are the disturbance source for lower-layer power smoothing. Table 1 reports the descriptive statistics of the hourly data.

Table 1 Descriptive Statistics of the Hourly Operating Data

Variable	Mean	Std. dev.	Min	Max	Median
Load	1.550	0.464	0.785	2.696	1.429
PV	2.255	3.627	0.000	11.933	0.000
Wind	0.493	0.278	0.000	1.122	0.527
RT price	0.209	0.090	0.092	1.346	0.190

As can be seen from Table 1, the standard deviation of PV output (3.627) is far larger than its mean (2.255), and its median is zero, which quantitatively confirms the diurnal intermittency; wind output has a mean of 0.493 and a standard deviation of 0.278 and fluctuates continuously; the load varies within 0.785–2.696 kW, with a peak-to-valley ratio of about 3.43. The real-time price averages 0.209 \$/kWh but reaches a maximum of 1.346 \$/kWh, giving a peak-to-valley ratio of about 14.58; the price fluctuation is significantly larger than that of the load, which provides a strong economic incentive for peak shaving and price arbitrage by storage. In actual operation, renewable forecasts inevitably contain errors; this paper characterizes the uncertainty intensity by the forecasting-error level ε (several levels from 5% to 40%) and injects it as a disturbance into the lower smoothing layer, so as to examine the smoothing capability of hybrid storage under different uncertainty levels.

2.3 Hybrid Energy Storage Model

The hybrid energy storage system consists of lithium-ion batteries and supercapacitors. The battery state of charge SOC_t describes its storage level, and its discrete state equation is:

$$SOC_{t+1}=SOC_t-\frac{P_t^b\Delta t}{E_{cap}}\times 100\% \tag{3}$$

where E_{cap} is the rated battery capacity, Δt the time step and P_t^b the battery power. According to the engineering parameters, the battery is a lithium-ion battery with a rated capacity E_{cap}=12 kWh, a power constraint $P_t^b \in [-4,4]$ kW

and an SOC operating range [SOC_{min},SOC_{max}]=[10%,90%]; the unit price is 600 \$/kWh, giving a total price of 7200. The SOC limits prevent overcharging and over-discharging and constitute a hard constraint that slows battery degradation. The supercapacitor is used to undertake the high-frequency power smoothing task of the lower layer. Its storage level is also described by a state of charge whose state equation has the same form as Eq. (3), but with small capacity, high power and fast response: the supercapacitor has a capacity of 1 kWh, a power limit of 10 kW and an initial SOC of 50%. In the two-layer framework, the supercapacitor does not participate in the upper-layer energy-type economic dispatch; it only absorbs, in the lower layer, the high-frequency deviations that arise when the battery tracks the upper-layer reference, thereby freeing the battery from frequent small-amplitude charging and discharging. The key parameters of the system and the storage are summarized in Table 2.

Table 2 Key Parameters of the Microgrid and the Hybrid Energy Storage System

Parameter	Value	Description
Battery type / capacity	Li-ion / 12kWh	Energy-type storage
Battery lifetime parameters [A, b]	[5000, 2]	Degradation cost modeling
Battery power constraint	[−4, +4]kW	Charge −4, discharge +4
Battery price / total price	600\$/kWh / 7200	Degradation cost conversion
Battery SOC range	[10%, 90%]	Prevents overcharge / over-discharge
Supercapacitor capacity / power	1kWh / 10kW	Power-type storage
Initial supercapacitor SOC	50%	Lower-layer smoothing
Grid power constraint	[−5, 10]kW	Sell −5, buy 10

2.4 Battery Degradation Cost Model

The battery degradation cost is a key component of the economic objective in this paper. The cycle life of a lithium-ion battery is closely related to the depth of discharge, and frequent, deep charging and discharging accelerate capacity fade. To convert lifetime loss into an economic quantity that can be added to the purchase cost, this paper adopts a degradation cost model related to the cumulative throughput. Let A and b be the battery lifetime parameters and C_{tot} the total battery price; then the degradation cost coefficient per unit throughput κ is defined as:

$$\kappa=\frac{C_{tot}}{2AE_{cap}^{b}} \tag{4}$$

Substituting C_{tot}=7200, A=5000, E_{cap}=12kWh and b=2 yields κ = 0.005 \$/(kWh)^2. Note that κ is not a price per unit of throughput: it is the coefficient of the b-th-power throughput model, so with b=2 it carries the unit \$/(kWh)^2 and the marginal cost of one more kWh of throughput grows with the depth already accumulated in the current half-cycle. Eq. (4) shows that the total battery price is amortized jointly by the lifetime parameter A and the b-th power of the capacity. In each dispatch period the degradation cost is the increment accrued over that period, which reads:

$$\begin{cases} C_t^{deg}=\kappa[(|S_t|+|P_t^b|\Delta t)^b-|S_t|^b], & S_tP_t^b>0 \\ C_t^{deg}=\kappa|P_t^b\Delta t|^b, & S_tP_t^b<0 \end{cases} \tag{5}$$

Eq. (5) shows that the marginal degradation cost of charging or discharging is $2\kappa|S_t|$, i.e. it grows with the depth already accumulated in the current half-cycle, and that each reversal of the power direction starts a new half-cycle from zero. The optimizer is therefore braked not only in proportion to how much it cycles but, more strongly, in proportion to how deep each swing is, which is the behaviour desired when chasing price spreads and tends to reduce unnecessary charging and discharging, thereby internalizing lifetime loss into the economic decision. This treatment is consistent with the idea of internalizing the degradation cost into a two-layer EMS in [11]; the difference is that [11] models degradation based on the depth of discharge and cycle life, whereas this paper adopts a throughput-based model that is quadratic in the depth of each half-cycle (b = 2), so that the marginal cost of throughput grows with the depth already accumulated in the current half-cycle; the coefficient is calibrated to the battery parameters of this project, so that a full-depth half-cycle of 12 kWh costs 0.72 \$ and 5000 full cycles amortise the total price of 7200 \$.

3 TWO-LAYER ENERGY MANAGEMENT AND DISPATCH MODEL BASED ON MPC

3.1 Overall Framework of the Two-Layer MPC

Microgrid energy management must answer two questions on distinctly different time scales: at the hourly scale, when to charge/discharge and when to interact with the grid in pursuit of economy; at the minute scale, how to suppress renewable fluctuations so as to guarantee power quality. A single-layer MPC can hardly handle both, because economic optimization requires a relatively long prediction horizon whereas fluctuation smoothing requires a very short control period. Therefore, this paper constructs a framework in which an upper and a lower MPC layer cooperate, as shown in Figure 2.

The upper economic dispatch layer works on a slow hourly time scale, solving in a rolling manner over a 48-step prediction horizon for the economically optimal reference plan of battery charging/discharging and grid interaction, and issues the reference power to the lower layer; the lower power smoothing layer works on a fast minute-level time scale, tracking the reference issued by the upper layer over a 12-step short horizon while calling on the supercapacitor to absorb the high-frequency deviations introduced by renewable forecasting errors, and feeds the actually executed SOC and power back to the upper layer for the next rolling round. The two layers are interfaced through the parameter from_fst = 2, i.e. the lower layer starts executing from the second upper-layer period reference, which aligns the cross-scale information

flow. This division of labour, in which the upper layer sets the plan and the lower layer guarantees execution, allows economy and power quality to be optimized separately at their appropriate time scales, while the two are coupled into a closed loop through the reference and the feedback.

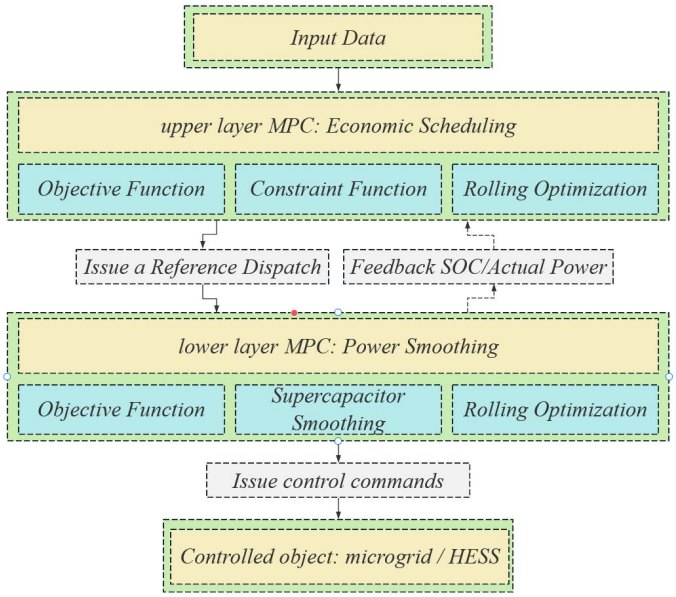


Figure 2 Framework of the Two-Layer MPC Energy Management

3.2 Upper-Layer Economic Dispatch Model

The optimization objective of the upper economic dispatch layer is to minimize, over the prediction horizon N_u=48, the sum of the electricity purchase cost and the battery degradation cost. Let k=0,1,…,N_u−1 be the period index within the prediction horizon, π_{t+k} the electricity price, P^g_{t+k} the grid power and P^b_{t+k} the battery power; then the upper-layer objective function is:

$$J_{up} = \sum_{k=0}^{N_u-1} [\pi_{t+k} f(P^g_{t+k}) \Delta t + \kappa((|S_{t+k}| + |P^b_{t+k}|\Delta t)^b - |S_{t+k}|^b)] \quad (6)$$

where the first term is the purchase/sale cost and the second term is the degradation cost, κ = 0.005 \$/(kWh)^2 is the degradation coefficient calibrated in Eq. (4), and purchasing and selling are priced asymmetrically: purchasing ($P^g > 0$) is settled at the full price and selling ($P^g < 0$) at a discount factor of 0.8, i.e.

$$f(P^g) = P^g (P^g > 0)$$
$$f(P^g) = 0.8 P^g (P^g < 0) \quad (7)$$

The selling discount factor of 0.8 reflects the actual market rule that the feed-in tariff is lower than the purchase tariff, preventing the optimizer from unbounded buy-low-sell-high arbitrage. The upper-layer optimization is subject to the following constraints: power balance, battery power, SOC, grid power and the SOC state equation. Since the power balance is an equality constraint, the grid power can be analytically back-substituted from $P^g_{t+k} = P^{net}_{t+k} - P^b_{t+k}$, and each upper-layer step uses only the battery power P^b_{t+k} as the decision variable, forming a nonlinear programming problem with SOC path constraints.

3.3 Receding-Horizon Optimization and Solution

The core of MPC lies in receding-horizon optimization and feedback correction. At the current instant t, the upper layer solves the optimization problem defined in Eq. (6) based on the latest SOC measurement and the net-load and price forecasts for the next N_u steps, obtaining an optimal control sequence $\{P^{b*}_t, P^{b*}_{t+1}, \ldots, P^{b*}_{t+N_u-1}\}$; however, only the first step P^{b*}_t is executed, after which the horizon is shifted forward by one step and the problem is re-solved at instant t+1 with the updated state. This cycle of predict-optimize-execute-feedback-re-predict can be described by the following iteration:

$$P^{b*}_t = \mathrm{argmin}_{P^b} J_{up}(P^b; SOC_t, \hat{P}^{net}_{t:t+N_u}, \hat{\pi}_{t:t+N_u}) \quad (8)$$

where $\hat{(\cdot)}$ denotes the predicted value. The optimization problem is solved by a sequential quadratic programming type of method with a convergence tolerance tol=10^{-8}. Horizon shifting and warm start are used in the rolling process: the optimal sequence of the previous instant is shifted by one position and used as the initial guess of the current solution, which markedly accelerates convergence. The feedback correction mechanism prevents forecast errors from accumulating; even if the prediction at one step is inaccurate, the next solution is re-corrected with the measured SOC, and this is precisely the fundamental advantage of MPC in dealing with uncertainty.

3.4 Lower-Layer Power Smoothing Model

The lower power smoothing layer works on a minute-level time scale. Its task is not to make economic decisions anew, but to smooth the high-frequency power fluctuations caused by renewable forecasting errors while tracking the upper-layer reference. Let N_l=12 be the lower-layer prediction horizon, P_{t+k}^{ref} the battery reference power issued by the upper layer and P_{t+k}^{b} the actual lower-layer battery power; then the lower-layer objective function is:

$$J_{low} = \sum_{k=0}^{N_l-1} [(P_{t+k}^{b}-P_{t+k}^{ref})^2+\kappa((|S_{t+k}|+|P_{t+k}^{b}|\Delta t)^b-|S_{t+k}|^b)] \quad (9)$$

The first term is a quadratic penalty on the tracking deviation, which keeps the lower layer from departing too far from the upper-layer economic plan; the second term is still the battery degradation cost, which suppresses unnecessary battery actions in the lower layer. The high-frequency power deficit caused by renewable forecasting errors is borne by the supercapacitor: the supercapacitor power P_{t+k}^{sc} fills the instantaneous gap between the actual net load and the battery-grid combination, so that the power balance of Eq. (1) still holds at the minute level. Owing to its small capacity, high power and fast response, the supercapacitor can absorb the high-frequency components that the battery cannot respond to in time, thereby protecting the battery from frequent small-amplitude charging and discharging. The lower layer is likewise subject to the supercapacitor SOC and power constraints and is executed in a rolling manner: Eq. (9) is solved in each minute-level control period, the first step is executed, and the actual states of the supercapacitor and the battery are fed back before rolling on.

3.5 Overall Algorithm Flow

Nesting the rolling optimizations of the upper and lower layers yields the complete two-layer MPC closed-loop dispatch algorithm, which performs the following steps at each hourly instant. Step 1: the upper layer reads the current SOC and the net-load and price forecasts and solves the economic dispatch problem of Eq. (6) to obtain the reference power sequences of the battery and the grid. Step 2: the reference is issued to the lower layer, which solves the tracking-and-smoothing problem of Eq. (9) in each minute-level period within that hour, calls on the supercapacitor to absorb high-frequency deviations and executes the control. Step 3: the actual power and SOC are recorded and the horizon is shifted by one step. The above process is repeated until the end of the simulation window, and the complete closed-loop dispatch results are output. The key parameters of the upper- and lower-layer MPC are summarized in Table 3.

Table 3 Key Parameters of the Upper- and Lower-Layer MPC

Parameter	Upper layer (economic dispatch)	Lower layer (power smoothing)
Time scale	Hourly	Minute-level
Prediction horizon	48	12
Iteration steps	48	12
Interface parameter from_fst	—	2
Optimization objective	min purchase + degradation cost	min tracking deviation + degradation cost
Solution tolerance	10^{-8}	10^{-8}
Primary storage	Battery	Supercapacitor

4 SIMULATION ANALYSIS

4.1 Simulation Setup and Data

The simulation is based on a real microgrid operating dataset. The hourly data consist of three columns, namely load, PV and wind, with 744 samples in total, and the real-time price is a single-column series of the same length; the minute-level data are the real 5-minute output waveforms of PV and wind, used to extract the high-frequency fluctuations around the hourly mean. The closed-loop simulation window is set to 48 h in accordance with the engineering parameters, with a 48-step upper-layer prediction horizon and a 12-step lower-layer horizon, and the battery and system parameters strictly follow the values in Table 2 of Section 2. To reproduce the smoothing capability of the lower layer under different uncertainty levels, the minute-level high-frequency waveforms are scaled by the forecasting-error level $\varepsilon \in \{5\%, 10\%, 20\%, 30\%, 40\%\}$ before injection. The upper-layer economic dispatch solves a constrained nonlinear program and the lower layer a quadratic tracking problem, both by the SLSQP method with a convergence tolerance 10^{-8}.

4.2 Characteristics of Renewable Output and Load

As shown in Figure 3, the three power series exhibit distinct temporal characteristics. The load curve shows fairly regular intraday peak-valley fluctuations, oscillating around a mean of 1.55 kW with a peak-to-valley ratio of about 3.43. PV output exhibits strong diurnal intermittency: it climbs rapidly with solar irradiance during the day, peaks around noon and drops to zero at night, with a zero-value proportion as high as 58.2%. Wind output is continuously available and fluctuates relatively gently, with a standard deviation of 0.278, and complements PV at night. The strong stochasticity and intermittency of renewable output cause the net load of the microgrid to fluctuate substantially in time, so that power balance cannot be maintained by source-side regulation alone; coordinated dispatch of storage and the main grid is

indispensable, which constitutes the practical need for the upper-layer economic dispatch and the lower-layer power smoothing that follow.

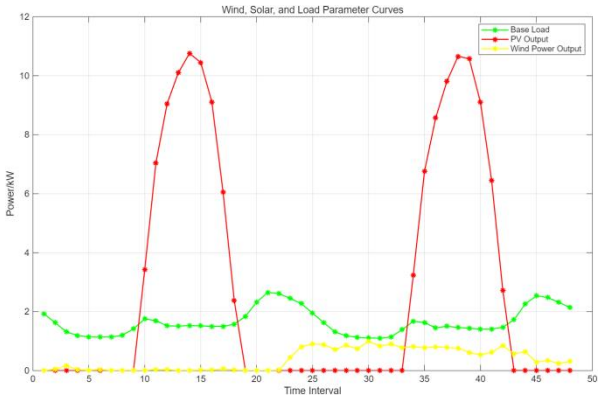


Figure 3 Load, PV and Wind Power Output Curves

4.3 Upper-Layer Economic Dispatch Results

The core objective of the upper-layer economic dispatch is to achieve peak shaving, valley filling and arbitrage by exploiting the time-varying price while satisfying the power balance and storage safety constraints. The grid interaction power and the electricity price show a clear inverse relationship: when the price is at its valley, the microgrid purchases more power and charges the battery; when the price is at its peak, it reduces purchases and even discharges the battery back to the grid. The statistics show a correlation coefficient of −0.620 between the price and the grid interaction power, quantitatively confirming the arbitrage behaviour of buying more at low prices and less or selling back at high prices. In terms of energy, the battery cumulatively charges 19.92 kWh at low prices and discharges 22.30 kWh at high prices within the simulation window, so the charging and discharging timing is highly consistent with the price, realizing typical peak shaving and valley filling. Figure 4 further shows the coupling between the storage dispatch power and the SOC.

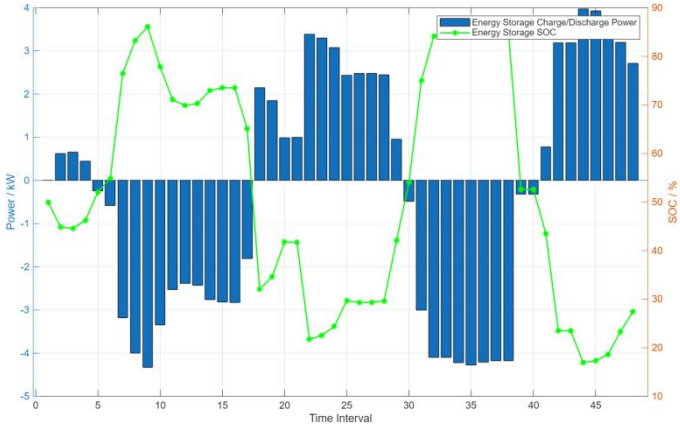


Figure 4 Coupling between the Storage Dispatch Power and the Battery SOC

As shown in Figure 4, the battery SOC rises and falls with the charging/discharging power: the SOC increases during charging periods and decreases during discharging periods, and the two are dynamically coupled. It is worth emphasizing that throughout the 48-hour closed loop the battery SOC operates strictly within the safe range of [10%, 90%], with a mean SOC of 53.6% and zero violations, which verifies the effectiveness of the nonlinear SOC path constraint in the receding-horizon optimization. The occasional reaching of the 10% or 90% boundary is the normal behaviour of the optimizer attaining an optimum on a constraint boundary, not a violation.

Figure 5 shows the balance between the upper-layer generation and the grid power. The upper-layer generation output and the grid interaction power jointly satisfy the net load demand in every period: when renewable output is abundant, the grid power decreases and may even turn into power sales; when renewable output is insufficient, the grid power increases to cover the deficit, and the two maintain the power balance in a complementary manner.

Figure 6 shows the operation of the battery power within its constraints. Throughout the dispatch process the battery power is strictly confined to the range of [−4, +4] kW without any violation. The standard deviation of the battery power is 1.590 kW, indicating that under the degradation cost the battery charges and discharges rather moderately and smoothly, avoiding frequent, large-amplitude cycling in pursuit of small price spreads. Taken together, Figures 4-6 show that the upper-layer economic dispatch effectively exploits the time-varying price to accomplish peak shaving, valley filling and arbitrage while guaranteeing power balance and storage safety; the total cost within the simulation window is 22.198 $, of which the purchase cost is 21.356 $ and the degradation cost 0.841 $, accounting for 3.79% of the total, so the degradation term is effectively internalized without becoming dominant.

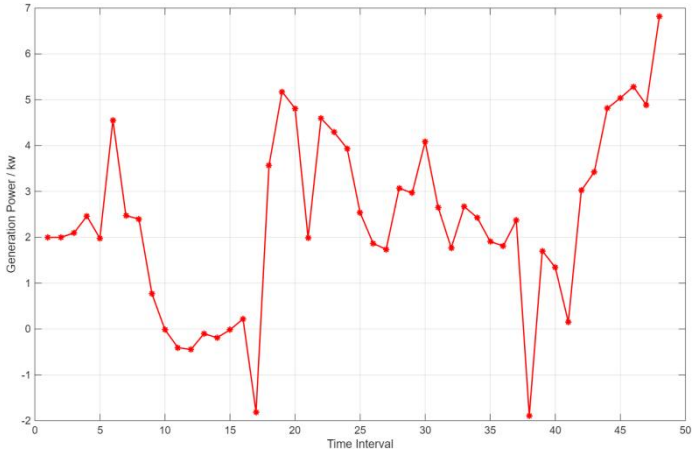


Figure 5 Upper-Layer Generation and Grid Interaction Power Curves

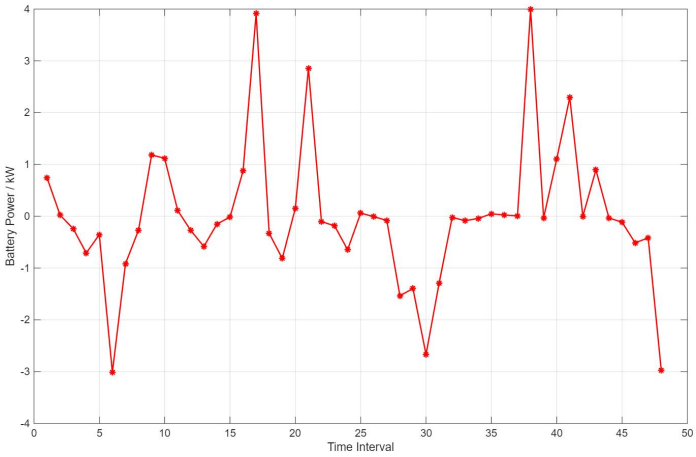


Figure 6 Battery Charging/Discharging Power Curve

4.4 Lower-Layer Power Smoothing Results

The task of the lower power smoothing layer is to suppress the high-frequency fluctuations caused by renewable forecasting errors with the supercapacitor while tracking the upper-layer economic plan. Figures 7 and 8 compare the SOC trajectories and the charging/discharging power of the two layers, respectively.

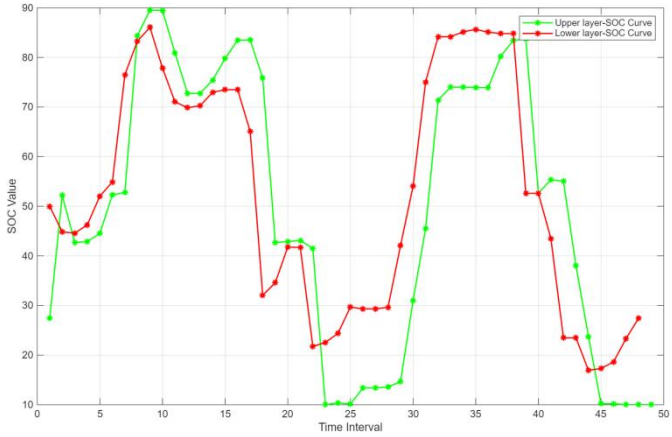


Figure 7 Comparison of the Upper- and Lower-Layer Battery SOC Trajectories

As shown in Figure 7, the upper-layer SOC trajectory reflects the economically optimal energy dispatch plan and is relatively smooth; the lower-layer SOC trajectory superimposes fine adjustments for high-frequency disturbances on top of tracking the upper layer, and its overall trend agrees with that of the upper layer, indicating that the lower layer faithfully follows the upper-layer economic plan while smoothing fluctuations, without significant deviation.

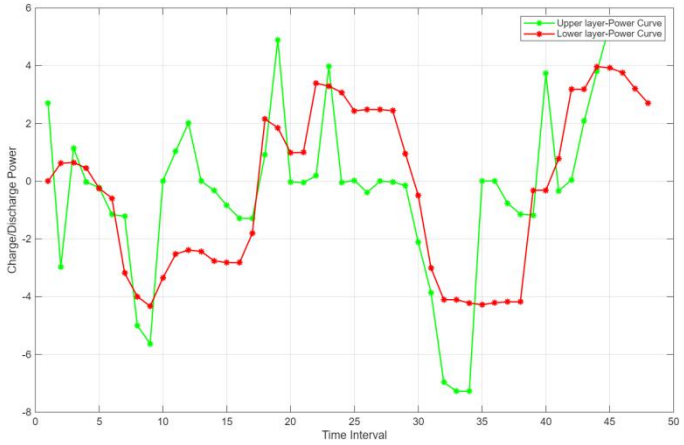


Figure 8 Comparison of the Upper- and Lower-Layer Battery Charging/Discharging Power

Figure 8 further compares the charging/discharging power of the two layers. The upper-layer power is an hourly step-type reference, whereas the lower-layer power exhibits fine minute-level tracking on that basis; the two agree closely in trend but differ in detail, and this difference is precisely the power adjustment made by the lower layer to smooth forecasting errors. To quantitatively evaluate the smoothing capability of hybrid storage under different forecasting-error levels, Table 4 compares the smoothing performance of HESS (battery plus supercapacitor) and battery-only modes. The smoothing advantage of hybrid storage increases monotonically with the forecasting error. At a 5% forecasting error, since the high-frequency component is inherently small, the standard deviation of the battery power is almost the same for HESS and the battery-only mode, with a reduction of −0.4% and a ramp-RMS reduction of only 1.0%; as the error rises to 20%, the reduction in the battery power standard deviation rises to 2.3% and the ramp reduction to 20.8%; at 40% error, the power standard deviation of the battery-only mode rises to 1.767 kW while that of the HESS mode remains at 1.574 kW, giving a standard-deviation reduction of 10.9% and a ramp-RMS reduction as high as 41.2%. This pattern clearly indicates that the supercapacitor mainly absorbs the high-frequency power component caused by forecasting errors; the larger the error, the more intense the high-frequency fluctuation, the heavier the smoothing task borne by the supercapacitor, and the more pronounced its protective effect on the battery. This is fully consistent with the HESS division of labour in which the battery handles energy dispatch and the supercapacitor handles high-frequency smoothing, and it also verifies the engineering value of the lower smoothing layer in highly uncertain scenarios.

Table 4 Smoothing Metrics of HESS and Battery-Only Storage under Different Forecasting Errors

Forecasting error ε	Battery-only power std (kW)	HESS power std (kW)	Reduction in std	Reduction in ramp RMS
5%	1.568	1.574	−0.4%	1.0%
10%	1.572	1.574	−0.1%	5.8%
20%	1.611	1.574	2.3%	20.8%
30%	1.680	1.569	6.6%	32.9%
40%	1.767	1.574	10.9%	41.2%

4.5 Impact Analysis of the Degradation Cost

To reveal the influence of the degradation cost on the dispatch strategy, this section compares two upper-layer strategies, one accounting for the degradation cost (this paper) and one ignoring it (baseline); the two are identical in all respects except whether the degradation term is included in the optimization objective, and the degradation cost is always accounted for truthfully according to Eq. (5). Because the cost is quadratic in the depth of each half-cycle, it cannot be recovered by multiplying the cumulative throughput by κ: writing $C_{deg} = \kappa \Sigma_i d_i^2$ and dividing by the throughput gives an effective unit degradation cost of $\kappa \cdot \bar{d}_w$, where $\bar{d}_w = \Sigma d_i^2 / \Sigma d_i = 3.81$ kWh (31.8% of the 12 kWh capacity) for the proposed strategy and 6.17 kWh (51.4%) for the baseline, i.e. 0.019 \$/kWh and 0.031 \$/kWh rather than κ itself. The increase of $\bar{d}_w$ from 3.81 to 6.17 kWh is the quantitative statement that the baseline does not merely cycle more (78.94 against 44.19 kWh), it cycles deeper. As shown in Table 5, the baseline strategy that ignores degradation has a purchase cost of 21.236 \$ but a degradation cost as high as 2.435 \$, giving a total cost of 23.671 \$; the proposed strategy that accounts for degradation has a purchase cost of only 21.356 \$, a marginal increase of 0.12 \$, while its degradation cost drops sharply to 0.841 \$, a reduction of 65.4%, and the total cost falls to 22.198 \$, a net saving of 1.473 \$, equivalent to a 6.2% reduction in total cost. More importantly, the storage lifetime is improved: under the proposed strategy the cumulative battery throughput is 44.19 kWh, 44.0% lower than the 78.94 kWh of the baseline, and the standard deviation of the battery power decreases from 2.340 kW to 1.590 kW, a reduction of 32.1%. This shows that the degradation-aware strategy buys a markedly smoother and more battery-friendly operating pattern at an almost negligible increase in purchase cost; restrained by the degradation term, the optimizer no longer cycles the battery frequently and heavily to chase small price spreads but uses it more conservatively, improving economy and lifetime simultaneously.

Table 5 Comparison between the Degradation-Aware and Degradation-Ignoring Strategies

Indicator	Degradation-aware (this paper)	Degradation-ignoring (baseline)	Change
Purchase cost ($)	21.356	21.236	+0.57%
Degradation cost ($)	0.841	2.435	−65.4%
Total cost ($)	22.198	23.671	−6.2%
Degradation cost share	3.79%	10.29%	—
Cumulative battery throughput (kWh)	44.19	78.94	−44.0%
Battery power std (kW)	1.590	2.340	−32.1%
Σd^2 (kWh²)	168.2	487.0	−65.5%
Weighted mean half-cycle depth $\bar{d}_w$ (kWh)	3.81	6.17	−38.3%
Effective unit degradation cost ($/kWh)	0.0190	0.0308	−38.3%

4.6 Robustness Test

To examine the sensitivity of the model to key parameters, a robustness analysis is carried out along two dimensions, namely the prediction horizon and the degradation weight. Table 6 reports the operating indices under different upper-layer prediction horizons.

Table 6 Sensitivity to the Upper-Layer Prediction Horizon

Prediction horizon	Total cost ($)	SOC violations	Cumulative throughput (kWh)
24	22.144	0	44.42
36	22.219	0	41.19
48 (this paper)	22.198	0	44.19

When the prediction horizon varies among 24, 36 and 48 steps, the total cost fluctuates only within a very narrow range of 22.144–22.219 $, a variation of less than 0.4%, and the number of SOC violations is always zero, indicating that the model is insensitive to the choice of prediction horizon and has good robustness. This means that in practical deployment the prediction horizon can even be shortened to reduce the computational burden without significantly compromising economy.

Table 7 Sensitivity to the Degradation Weight

Degradation weight w	Total cost ($)	Cumulative throughput (kWh)	Power std (kW)
0.0 (no degradation)	23.671	78.94	2.340
0.5	22.399	51.07	1.792
1.0 (this paper)	22.198	44.19	1.590
2.0	22.212	33.83	1.361

Table 7 further examines the influence of the degradation weight on dispatch behaviour. As the degradation weight increases from 0 to 2, the cumulative battery throughput decreases monotonically from 78.94 kWh to 33.83 kWh and the power standard deviation decreases monotonically from 2.340 kW to 1.361 kW. This monotonic relationship agrees fully with physical intuition: a larger degradation penalty induces the optimizer to use the battery more conservatively and to reduce unnecessary throughput. The result also indirectly verifies the correctness of the degradation cost model, since the degradation term indeed plays the expected braking role in dispatch decisions, and its strength is smoothly adjustable with the weight, providing operators with a tunable knob to trade off economy against lifetime.

5 DISCUSSION

5.1 Advantages and Applicability of the Method

Taking the simulation results of Section 4 together, the advantages of the proposed two-layer MPC-HESS dispatch model are reflected at three levels. The first is the capability of cross-time-scale coordination. The upper layer optimizes economy over a 48-step hourly horizon and the lower layer guarantees power quality over a 12-step minute-level horizon, and the two are coupled into a closed loop through the reference and the feedback. This hierarchical structure allows economic optimization and fluctuation smoothing to work at their appropriate time scales, avoiding the dilemma of single-layer MPC in which a long horizon cannot be computed fast and a short horizon cannot see far, and it continuously corrects forecast errors through rolling feedback, so it is inherently robust to renewable uncertainty, as confirmed by the prediction-horizon robustness in Table 6. The second is the internalization of the degradation cost. After the battery degradation cost is explicitly modeled on the basis of throughput and embedded in the economic objective, the optimizer is naturally restrained when pursuing price arbitrage; compared with the baseline strategy that ignores degradation, it achieves synergistic improvements of a 44.0% reduction in throughput, a 32.1% reduction in power fluctuation and a 6.2% reduction in total cost, showing that economy and lifetime are not in conflict and can be optimized in the same direction under appropriate modeling. The third is the rational division of labour of hybrid storage. Assigning low-frequency energy dispatch to the battery and high-frequency fluctuation smoothing to the supercapacitor is particularly effective under high

forecasting errors; at 40% error the ramp-RMS reduction of the battery reaches 41.2%, verifying the engineering value of HESS over battery-only storage under uncertainty.

In terms of applicability, the model applies to grid-connected microgrids with PV, wind and hybrid storage, and is particularly suitable for scenarios with a large price peak-to-valley difference, a high renewable penetration and sensitivity to storage lifetime. The model is insensitive to the prediction horizon, which facilitates deployment on embedded controllers with limited computing resources; the adjustable degradation weight also allows operators to trade off economy against lifetime protection flexibly according to the remaining battery life and the price market.

5.2 Limitations and Outlook

This study still has several limitations that point to directions for future improvement:

(1) Model performance depends on the accuracy of renewable output and price forecasts. Although rolling feedback in this paper mitigates the accumulation of forecast errors and the robustness of the lower layer is tested over several error levels from 5% to 40%, explicit stochastic or robust optimization has not yet been introduced to systematically characterize the probability distribution of uncertainty; this is a direction that can be deepened in future work.

(2) This paper focuses on the battery degradation cost and approximates the supercapacitor as an ideal power source without degradation; practical supercapacitors also age with cycling, and their degradation could be incorporated into the lower-layer objective in future work so as to characterize the whole-life cost of hybrid storage more completely.

(3) This paper addresses a single microgrid and does not consider the coordination of flexible resources such as interconnected microgrids, demand response and electric vehicles; extending the two-layer framework to cooperative dispatch of multiple microgrids is a valuable extension.

(4) The simulation window is set to 48 h to match the engineering parameters; although this is sufficient to cover a complete intraday price cycle, operation assessment over longer time scales remains to be supplemented.

6 CONCLUSIONS

To address the dual challenges that renewable uncertainty and battery degradation pose to the economic operation of microgrids, this paper proposes and validates a two-layer energy management and dispatch model for microgrid hybrid energy storage systems based on model predictive control. The upper economic dispatch layer minimizes the sum of the purchase and degradation costs over a 48-step receding horizon and explicitly internalizes the battery degradation cost, modelled as a quadratic function of the depth of each half-cycle ($b = 2$), into the economic objective; the lower power smoothing layer tracks the upper-layer reference over a 12-step short horizon and uses the fast-responding supercapacitor to smooth the high-frequency fluctuations caused by renewable forecasting errors. A 48-hour closed-loop simulation based on real hourly data containing PV and wind generation and a real-time price shows that: the upper-layer dispatch achieves price-driven peak shaving and valley filling, and the battery SOC operates strictly within [10%, 90%] with zero violations; compared with the baseline strategy that ignores degradation, the degradation-aware strategy reduces the cumulative battery throughput by 44.0%, the standard deviation of power fluctuation by 32.1% and the total cost by 6.2%, achieving a synergistic improvement of economy and lifetime; the lower-layer supercapacitor raises the ramp-RMS reduction of the battery power to 41.2% at a 40% forecasting-error level, and the smoothing benefit becomes more pronounced as the error increases; the two tests of prediction-horizon sensitivity and degradation-weight monotonicity further verify the robustness of the model. In summary, the proposed two-layer MPC-HESS model can coordinate the operational economy, power quality and storage lifetime of a microgrid while ensuring supply balance and storage safety, providing a practical hierarchical scheduling method for the optimal operation of microgrids with hybrid energy storage under uncertainty.

COMPETING INTERESTS

The authors have no relevant financial or non-financial interests to disclose.

FUNDING

This paper presents the research findings of the university-level research project at Yinchuan College of Energy titled “A Study on a Two-Layer Energy Management and Dispatch Model for Microgrids and HESS Based on MPC” (2024-KY-Y-10).

REFERENCES

[1] Feng B, Yang H, Yang Q, et al. Multi-period stochastic economic dispatch of microgrid considering renewable energy uncertainty using parallel algorithm. 2019 IEEE Innovative Smart Grid Technologies - Asia (ISGT Asia). IEEE, 2019: 3185-3189.

[2] Xie P, Guerrero J M, Tan S, et al. Optimization-based power and energy management system in shipboard microgrid: A review. IEEE Systems Journal, 2022, 16(1): 578-590.

[3] Schwenzer M, Ay M, Bergs T, et al. Review on model predictive control: an engineering perspective. The International Journal of Advanced Manufacturing Technology, 2021, 117(5-6): 1327-1349.

[4] Pippia T, Sijs J, De Schutter B. A single-level rule-based model predictive control approach for energy management of grid-connected microgrids. IEEE Transactions on Control Systems Technology, 2020, 28(6): 2364-2376.
[5] Ponce G, Mandal P, Galvan E. Integration of battery energy storage dispatch using model predictive control for a hybrid microgrid energy management system. 2023 IEEE Industry Applications Society Annual Meeting (IAS). IEEE, 2023: 1-7.
[6] Nair U R, Costa-Castelló R. An analysis of energy storage system interaction in a multi objective model predictive control based energy management in DC microgrid. 2019 24th IEEE International Conference on Emerging Technologies and Factory Automation (ETFA). IEEE, 2019: 739-746.
[7] Liu S, Ling R. Power allocation control method for hybrid energy storage system of lithium ion battery and supercapacitor. 2020 32nd Chinese Control and Decision Conference (CCDC). IEEE, 2020: 1346-1350.
[8] Chen T H, Liao R N, Yang C Y, et al. Application of grid-level battery energy storage system to wind power fluctuation smoothing. Journal of Clean Energy Technologies, 2016, 4(3): 201-204.
[9] Jiang S, Peng C. Hierarchical control of microgrid with multi distributed generations. 2018 5th IEEE International Conference on Cloud Computing and Intelligence Systems (CCIS). IEEE, 2018: 142-145.
[10] Guo X, Gu F, Liu H, et al. Sustainable PV-hydrogen-storage microgrid energy management using a hierarchical economic model predictive control framework. Energy Informatics, 2025, 8(1): 18.
[11] Ju C, Wang P, Goel L, et al. A two-layer energy management system for microgrids with hybrid energy storage considering degradation costs. IEEE Transactions on Smart Grid, 2018, 9(6): 6047-6057.